

# The Structure of a Human p110 $\alpha$ /p85 $\alpha$ Complex Elucidates the Effects of Oncogenic PI3K $\alpha$ Mutations

Chuan-Hsiang Huang,<sup>1,3</sup> Diana Mandelker,<sup>2</sup> Oleg Schmidt-Kittler,<sup>2</sup>  
Yardena Samuels,<sup>2\*</sup> Victor E. Velculescu,<sup>2</sup> Kenneth W. Kinzler,<sup>2</sup>  
Bert Vogelstein,<sup>2†</sup> Sandra B. Gabelli,<sup>1†</sup> L. Mario Amzel<sup>1†</sup>

*PIK3CA*, one of the two most frequently mutated oncogenes in human tumors, codes for p110 $\alpha$ , the catalytic subunit of a phosphatidylinositol 3-kinase, isoform  $\alpha$  (PI3K $\alpha$ , p110 $\alpha$ /p85). Here, we report a 3.0 angstrom resolution structure of a complex between p110 $\alpha$  and a polypeptide containing the p110 $\alpha$ -binding domains of p85 $\alpha$ , a protein required for its enzymatic activity. The structure shows that many of the mutations occur at residues lying at the interfaces between p110 $\alpha$  and p85 $\alpha$  or between the kinase domain of p110 $\alpha$  and other domains within the catalytic subunit. Disruptions of these interactions are likely to affect the regulation of kinase activity by p85 or the catalytic activity of the enzyme, respectively. In addition to providing new insights about the structure of PI3K $\alpha$ , these results suggest specific mechanisms for the effect of oncogenic mutations in p110 $\alpha$  and p85 $\alpha$ .

Phosphatidylinositol 3-kinases (PI3Ks) are lipid kinases that phosphorylate phosphatidylinositol 4,5-bisphosphate [PI(4,5)P<sub>2</sub> or PIP<sub>2</sub>] at the 3-position of the inositol ring, and thus generate phosphatidylinositol 3,4,5-trisphosphate (PIP<sub>3</sub>), which, in turn, initiates a vast array of signaling events. PI3Ks are heterodimers, composed of catalytic and regulatory subunits, that are activated by growth factor-receptor tyrosine kinases (1, 2). PIP<sub>3</sub> levels are tightly regulated by the action of phosphatases, such as the phosphatase and tensin homolog (PTEN) (3). PIP<sub>3</sub> produced by PI3Ks acts as a docking site for pleckstrin homology (PH)-containing proteins, such as the Akt serine-threonine kinases (4). Once at the membrane, Akt's are activated by phosphorylation at two sites and, in turn, phosphorylate numerous protein targets (5–17). The biological consequences of Akt activation are broad and include regulation of cell proliferation, survival, and motility (2, 18–20).

The PI3K pathway was first linked to cancer when Vogt and colleagues reported that the avian sarcoma virus 16 genome encodes an oncogene that is derived from a cellular PI3K gene (21).

<sup>1</sup>Department of Biophysics and Biophysical Chemistry, Johns Hopkins University School of Medicine, Baltimore, MD 21205, USA. <sup>2</sup>Ludwig Center for Cancer Genetics and Therapeutics, and Howard Hughes Medical Institute at the Johns Hopkins Kimmel Cancer Center, Baltimore, MD 21231, USA. <sup>3</sup>Graduate Program in Immunology, Johns Hopkins University School of Medicine, Baltimore, MD 21205, USA.

\*Present address: National Human Genome Research Institute, National Institutes of Health, Bethesda, MD 20892, USA.

†To whom correspondence should be addressed. E-mail: mamzel@jhmi.edu (L.M.A.); gabelli@jhmi.edu (S.B.G.); vogelbe@jhmi.edu (B.V.)

The finding that PTEN is inactivated by mutations in various tumors solidified the relevance of this pathway to human cancer (22–24). Other genetic alterations in pathway members have been identified, including occasional mutations in the regulatory subunit p85 of PI3K (25–32).

Particularly exciting was the more recent discovery that *PIK3CA*, the gene encoding the catalytic subunit of PI3K $\alpha$ , was somatically mutated in a significant fraction of diverse tumor types (33–41). Most of the reported mutations in *PIK3CA* cluster in conserved regions within the region coding for the helical and kinase domains of p110  $\alpha$  (33). As these mutations constitutively activate its kinase activity (42–48), the enzyme appears to be an ideal target for drug development. Indeed, several low-molecular-weight compounds that inhibit p110 $\alpha$  activity have been described (49). Most of these compounds, however, are not specific and inhibit other PI3Ks, as well as other kinases. Progress in this area of drug development would be facilitated by knowledge of the structure of the p110 $\alpha$ /p85 $\alpha$  complex.

The p110 $\alpha$  subunit of PI3K $\alpha$  has five domains: an N-terminal domain called ABD (adaptor-binding domain) that binds to p85 $\alpha$ , a Ras-binding domain (RBD), a domain called C2 that has been proposed to bind to cellular membranes, a helical domain of unknown function, and a kinase catalytic domain (Fig. 1A) (1, 2, 18, 19). In its basal state, the p110 $\alpha$  subunit is bound to and inhibited by the regulatory subunit p85 $\alpha$  or p85 $\alpha$ -related proteins. The p85 $\alpha$  polypeptide also has five known domains including two SH2 domains (the N-terminal nSH2 and C-terminal cSH2) separated by an inter-SH2 (iSH2) domain that binds to the catalytic subunit. When appropriate

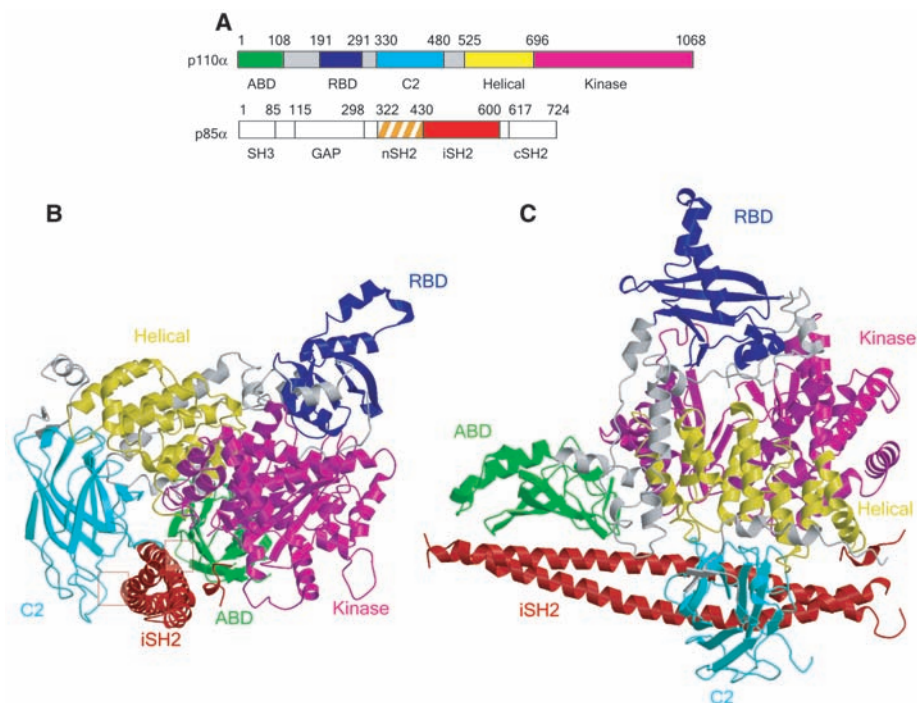


**Fig. 1.** Overview of the p110 $\alpha$ /nSH2 heterodimer. **(A)** Scheme of the domain organization. The same color coding is used throughout this article unless specified. Gray regions are linkers between domains. The nSH2 domain of p85 $\alpha$ , denoted by the region with orange stripes, was not traced in the final model but its location in the complex was determined as described in the text. **(B)** Ribbon diagram of the p110 $\alpha$ /nSH2 heterodimer. The iSH2 ABD and iSH2 C2 contacts are boxed. **(C)** Ribbon diagram of the p110 $\alpha$ /nSH2 heterodimer, alternate view.

cellular stimuli are present, the nSH2 and cSH2 domains bind phosphorylated tyrosines in activated receptors and adapter proteins, and this phosphotyrosine binding activates the p110 $\alpha$  catalytic subunit without releasing p85 $\alpha$  from p110 $\alpha$ .

Although the structures of pig and human p110 $\gamma$  are known (50–52), the sequence identity between p110 $\alpha$  and p110 $\gamma$  is only 35%. In addition, unlike p110 $\alpha$ , p110 $\gamma$  does not require binding to a regulatory subunit for its catalytic activity, and the reported structures of p110 $\gamma$  do not include the ABD domain. The crystal structure of a complex between the N-terminal ABD domain of p110 $\alpha$  (residues 1 to 108) and the human p85 $\alpha$  (iSH2) domain (residues 431 to 600) was recently determined (53). The structure of the isolated nSH2 domain has been previously reported (54). In the current study, we crystallized and determined the structure of a complex between the full-length human p110 $\alpha$  catalytic subunit and the domains of the p85 $\alpha$  regulatory subunit critical for its binding and activation.

**Results and Discussion.** In a baculovirus production system, we found that human p110 $\alpha$  was produced at easily detectable levels only when coexpressed with the regulatory p85 $\alpha$  protein. However, coexpression of p110 $\alpha$  with full-length p85 $\alpha$  led to protein aggregation. We tested different truncated versions of p85 $\alpha$ , all containing the iSH2 region, and found that residues 322 to 600 (termed niSH2) produced the highest protein yield. The complex was enzymatically active, with a Michaelis constant  $K_M$  of 11  $\mu$ M for adenosine triphosphate (ATP) and of 58  $\mu$ M for L- $\alpha$ -phosphatidylinositol. It contained all five p110 $\alpha$  domains (ABD, residues

1 to 108; RBD, residues 190 to 291; C2, residues, 330 to 480; helical, residues 525 to 696; and kinase, residues 697 to 1068), as well as the nSH2 (residues 322 to 430) and iSH2 (residues 431 to 600) domains of p85 $\alpha$  (Fig. 1A). The structure of the p110 $\alpha$ /niSH2 heterodimer was determined with data to 3.05  $\text{\AA}$  resolution and refined to an  $R_{\text{work}}/R_{\text{free}}$  of 26.3/32.3 (Table 1).

**Description of the structure.** The p110 $\alpha$ /niSH2 heterodimer has an overall triangular shape with the long coiled-coil of iSH2 forming the base (Fig. 1C). ABD, which is located near one end of the complex, contacts the iSH2 coiled-coil from the top, burying 2237  $\text{\AA}^2$  of surface area, while the C2 domain interacts with the iSH2 from the side and buries an additional 1233  $\text{\AA}^2$  (total buried surface area 3470  $\text{\AA}^2$ ) (Fig. 1B). The helical and kinase domains form the bulk of the center of the complex but are not in direct contact with iSH2. The RBD sits at the top corner, farthest away from the iSH2. Adventitiously, the N-terminal portion of the His-tag (residues –27 to –15; complete tag: residues –1 to –28) in the p110 $\alpha$  construct, which was not removed before crystallization, is locked in a polar pocket between the RBD and the kinase domains of a neighboring molecule, which may contribute to the stability of the crystals.

ABD and RBD are both small globular domains of about 100 residues in length with an  $\alpha/\beta$ -sandwich topology. A long linker (residues 109 to 189) containing four helices connects these two domains. ABD displays a complex set of interactions with helix  $\alpha$ 1K of the kinase domain and helix  $\alpha$ 1L, which is part of the linker between ABD and RBD. The previously reported crystal structure of the ABD domain of p110 $\alpha$  in complex with the iSH2 of p85 did not reveal how ABD interacts with the rest of p110 $\alpha$  (53). Nevertheless, the contacts between the isolated ABD and iSH2 domains, as well as their relative orientations, are in agreement with those we found in the complex between the intact p110 $\alpha$  and niSH2.

The C2 domain is a  $\beta$  sandwich of two four-stranded antiparallel sheets. The linker between RBD and C2 is a long coil (residues 292 to 329) with a short helix near its N terminus. Part of this linker (residues 307 to 324), as well as the linker between the C2 and the helical domains (residues 506 to 527), were not traced because their density was not well defined. The C2 domain is the least conserved among the four common domains of class I PI3Ks, with only 27% sequence identity between p110 $\alpha$  and p110 $\gamma$ . Although the characteristic eight-stranded antiparallel  $\beta$ -sandwich topology is preserved, there are significant differences between the intervening loops of p110 $\alpha$  and p110 $\gamma$ . In particular, the loop connecting  $\beta$ 5C2 and  $\beta$ 6C2 in p110 $\alpha$  (CBR3, residues 406 to 424) is about 10 residues shorter than the corresponding loop in p110 $\gamma$ . As in the C2 domain of p110 $\gamma$ , CBR3 of p110 $\alpha$  contains basic residues Lys<sup>410</sup>, Arg<sup>412</sup>, Lys<sup>413</sup>, and Lys<sup>416</sup>, which appear

to be involved in the interaction with the lipid membrane. The reduced length of CBR3 in p110 $\alpha$  might be a consequence of the spatial constraint imposed by the interaction between C2 and iSH2.

One unexpected feature of the C2 domain in the p110 $\alpha$ /niSH2 crystal structure is its interaction with the iSH2 of p85. It had been suggested that the iSH2 coiled-coil sits in a groove between the C2 and kinase domains (53), but the exact position of iSH2 in the complex was not known. In the structure presented here, Asp<sup>560</sup> and Asn<sup>564</sup> of iSH2 are within hydrogen-bonding distance (2.8 and 3.0  $\text{\AA}$ ) of Asn<sup>345</sup> of C2 (Fig. 2C). This interaction, not identified in previous studies, forms an important additional contact between iSH2 and p110 $\alpha$ .

The helical domain folds as an all  $\alpha$ -helical structure. It was proposed to be the core of the molecule to which all other domains attach (52). In the p110 $\alpha$ /niSH2 structure, however, the main role of the helical domain within the p110 $\alpha$  subunit is to bridge the C2 and kinase domains, the only two domains with which it is in direct contact.

The kinase domain harbors the catalytic site of the enzyme. It is a two-lobed structure formed by two  $\alpha/\beta$  subdomains separated by a cleft, an architecture typical of protein and lipid kinases. In p110 $\alpha$ , the smaller N-terminal domain comprises residues 697 to 851 and the larger C-terminal domain residues 852 to 1068. On the basis of the structures of other protein kinases, the activation and catalytic loops of p110 $\alpha$  were assigned to residues 933 to 957 and 912 to 920, respectively (fig. S1). Residues 941 to 950 of the activation loop, as well as residues beyond 1050, were disordered and were not traced. The structure of this domain is highly conserved among class I PI3Ks, particularly for residues around the substrate-binding pocket situated between the N- and C-terminal lobes of the kinase domain. Alignment of the kinase domains of p110 $\alpha$  and p110 $\gamma$  shows a root mean square deviation (RMSD) of 1.8  $\text{\AA}$  between 288 out of 337 aligned C $\alpha$  atoms. Analysis of this alignment shows that the major deviation occurs at helix  $\alpha$ 12K (residues 1032 to 1048) with an RMSD of 3.2  $\text{\AA}$ . Alignment of the kinase domain without helix  $\alpha$ 12K shows a deviation of 1.6  $\text{\AA}$ . As discussed below, helix  $\alpha$ K12 contains two cancer-related mutations and is close to the activation loop, as well as the nSH2 domain of p85 $\alpha$ . This suggests that p85 $\alpha$  regulates p110 $\alpha$  activity through a helix  $\alpha$ K12-mediated conformational change of the activation loop.

To identify the ATP-binding site in p110 $\alpha$ , crystals were soaked in ATP-containing mother liquor solutions. Diffraction data, however, did not show density for the nucleotide. Analysis of the crystal structure provides an explanation: The ATP-binding site of p110 $\alpha$  participates in a crystal contact and is occupied by a loop (residues 226 to 239) from the RBD domain of a neighboring molecule (fig. S2). The architecture of the portions of p110 $\alpha$  that are present in the structure of the human p110 $\gamma$  are similar, despite the low

**Table 1.** Data collection and refinement statistics.

Measure	Value
<b>Data collection</b>	
X-ray source	BNL-X29( $\lambda = 1.0809 \text{ \AA}$ )
Space group	P2 <sub>1</sub> 2 <sub>1</sub> 2 <sub>1</sub>
Cell dimensions <i>a</i> , <i>b</i> , <i>c</i> ( $\text{\AA}$ )	115.1, 117.1, 151.6
Resolution ( $\text{\AA}$ )	3.05
Measured reflections	270,209
$R_{\text{sym}}$	7.2 (43.3)
$\langle I / \sigma \rangle$	9.4 (2.1)
Completeness (%)	98.7 (88.2)
Redundancy	7.1 (5.3)
<b>Refinement</b>	
Resolution ( $\text{\AA}$ )	46.4–3.05
No. reflections (work/test set)	36,888/2000
$R_{\text{work}}/R_{\text{free}}$	26.3/32.3
No. residues	1133
No. atoms of protein	9365
Average <i>B</i> -factor $\text{\AA}^2$	85.7
<b>RMSD</b>	
Bond lengths ( $\text{\AA}$ )	0.01
Bond angles ( $^\circ$ )	1.5

Highest-resolution shell is shown in parentheses.  $R_{\text{sym}} = \sum_{hkl} |I(hkl) - \langle I(hkl) \rangle| / \sum_{hkl} I(hkl)$ , where  $\langle I(hkl) \rangle$  is the mean of the symmetry-equivalent reflections of  $I(hkl)$ .

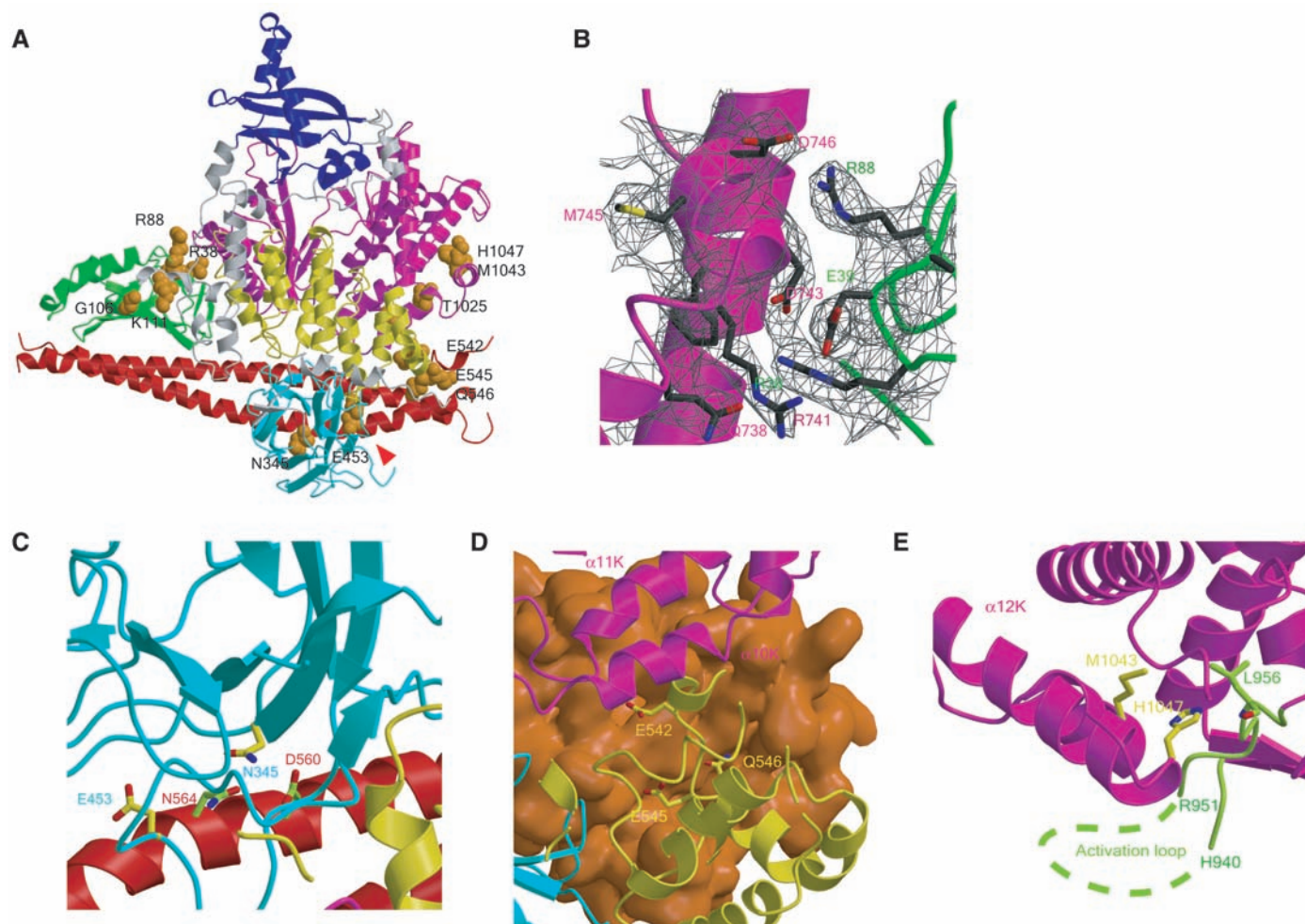


**Fig. 2.** Mutations in PIK3CA identified in human cancers. **(A)** Distribution of representative mutations within p110 $\alpha$ . Residues mutated in cancers are shown as CPK models. The start of the cancer-associated truncation (residue 571 of p85) is shown by the red arrowhead. **(B)** Electron density map of Arg<sup>38</sup> and Arg<sup>88</sup> cancer mutations shown at the interface between the ABD and the kinase domains. **(C)** Close-up view of the interface of the C2 domain of p110 with iSH2 of p85. The stick representation of the

Asn<sup>345</sup> mutation of C2 and the residues within iSH2 (Asp<sup>560</sup> and Asn<sup>564</sup>) with which it may interact are shown. **(D)** Mutations in the helical domain (Glu<sup>542</sup>, Glu<sup>545</sup>, and Gln<sup>546</sup>), located at the interface with nSH2 (orange surface). **(E)** Mutations of the kinase domain (Met<sup>1043</sup> and His<sup>1047</sup>), located near the C-terminal end of the activation loop, are shown in light green. The part of the activation loop between residues 941 and 950 could not be traced (see text).

sequence identity between the two proteins (fig. S1 and fig. S3) (52).

**Cancer-specific mutations.** Cancer-associated mutations have been identified in the ABD, C2, helical, and kinase domains of p110 $\alpha$  (33). The distribution of representative mutations within the p110 $\alpha$  structure is shown in Fig. 2A. Several of these mutations have been shown to result in enhanced enzymatic activity in vitro and in vivo (33, 42, 43). Mutations located in different domains were thought to act through unrelated mechanisms but this hypothesis was difficult to prove in the absence of structural information. The structure presented here sheds light on the mechanisms through which these mutations may affect kinase activity.

The ABD domain mutations (in which, for example, cysteine, histidine, and glutamine replace arginine at residue 38 and 88) Arg<sup>38</sup>Cys, Arg<sup>38</sup>His, and Arg<sup>88</sup>Gln were initially thought to disrupt the interaction between ABD and iSH2,

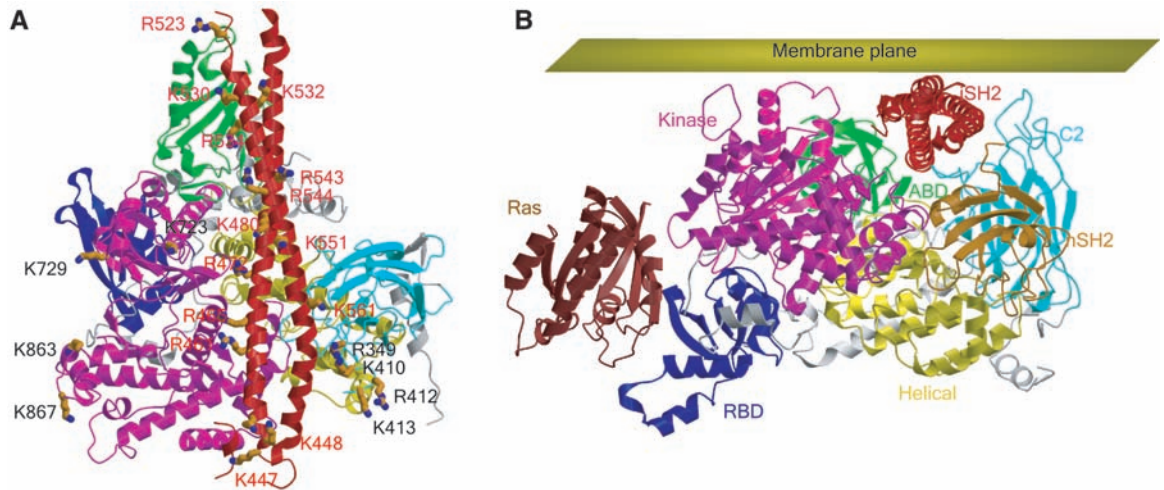
but were later found not to be located at the interface in a crystal structure of ABD in complex with iSH2 (53). The effect of these mutations, however, was not evident from the structure of ABD-iSH2 heterodimer. The structure of the p110 $\alpha$ /niSH2 reveals that both Arg<sup>38</sup> and Arg<sup>88</sup> are located at a contact between the ABD and the kinase domains, within hydrogen-bonding distance ( $<3.2$  Å) of Gln<sup>738</sup>, Asp<sup>743</sup>, and Asp<sup>746</sup> of the N-terminal lobe of the kinase domain (Fig. 2B). Mutations of Arg<sup>38</sup> and Arg<sup>88</sup> are likely to disrupt these interactions, resulting in a conformational change of the kinase domain that alters enzymatic activity.

Mutations in the C2 domain were thought to change the affinity of p110 $\alpha$  for the lipid membrane (47). In the structure reported here, Asn<sup>345</sup>, mutated to Lys in some cancers, is within hydrogen-bonding distance (2.8 Å and 3.0 Å) of Asn<sup>564</sup> and Asp<sup>560</sup> of iSH2 (Fig. 2C). This suggests that an Asn<sup>345</sup> mutation may disrupt the

interaction of the C2 domain with iSH2. This would presumably alter the regulatory effect of p85 on p110 $\alpha$ , rather than disrupt the interaction of p110 $\alpha$  with the lipid membrane. It is intriguing that another mutation identified in cancer, Glu<sup>545</sup>Gln, is also located at the interface between C2 and iSH2. The density for its side chain, however, is not defined well enough in the structure to identify a direct interaction.

The helical domain contains two residues, Glu<sup>542</sup> and Glu<sup>545</sup>, that are frequently mutated in cancers ("hot spots"). In the majority of cases, these two residues are mutated to Lys, causing a charge reversal. Glu<sup>542</sup> and Glu<sup>545</sup>, as well as the less frequently mutated Gln<sup>546</sup>, are located on an exposed region of the helical domain (Fig. 2A). Biochemical studies suggested that these residues interact with Lys<sup>379</sup> and Arg<sup>340</sup> of the p85 nSH2 domain and that this interaction inhibited the activity of the catalytic subunit (53, 55). Although nSH2 was included in our p110 $\alpha$ /niSH2 protein

**Fig. 3.** Model of membrane interaction. (A) Positively charged residues on the surface of iSH2 domain of p85 $\alpha$  (red) and loops of the C2 and kinase domains of p110 $\alpha$  (black) are proposed to contact the negatively charged phospholipid bilayer. (B) Model of p110 $\alpha$ /niSH2 bound to Ras and its proposed orientation with respect to the lipid membrane.



complex, it was not highly ordered in the crystal. A model of the complete p110 $\alpha$ /niSH2 complex was therefore created by placing the previously determined structure of the nSH2 domain of human p85 $\alpha$  (54) into the weak density of the final  $2F_{\text{obs}} - F_{\text{calc}}$  map of p110 $\alpha$ /niSH2, while taking into account the interactions identified biochemically (53). In this model, nSH2 is placed close to the interface between the kinase and the helical domain and interacts with both domains. This model is fully consistent with the biochemical experiments of Miled *et al.* (53) demonstrating that mutations at residues 542, 545, and 546 abrogate the inhibitory effect of nSH2 (Fig. 2D). Two ways in which the effects of these mutations are communicated to the complex can be identified: Mutations may modify the orientation of nSH2 with respect to the helical and the kinase domains, and by changing the interaction of the helical domain with nSH2, the mutations may alter the relative positions of helices  $\alpha$ 11K and  $\alpha$ 12K.

His<sup>1047</sup> in the kinase domain is another hot spot for somatic mutations in cancer. It is interesting that His<sup>1047</sup> is mutated to Arg in the majority of cases, yet arginine is normally present at the homologous position in human p110 $\gamma$  (fig. S1). In the structure of the p110 $\alpha$ /p85 complex, His<sup>1047</sup> is located within helix  $\alpha$ 12K of the C-terminal lobe of the kinase domain and is close to the C-terminal end of the activation loop, possibly forming a hydrogen bond with the main-chain carbonyl of Leu<sup>956</sup> within the activation loop (Fig. 2E). Mutations of His<sup>1047</sup> most likely have a direct effect on the conformation of the activation loop, changing its interaction with phosphatidylinositide substrates. Another less frequently observed mutation, Met<sup>1043</sup>Ile, is located on the same helix, and we hypothesize that it also exerts its effect through changes in the activation loop.

Although alterations of p85 $\alpha$  in cancers are much less common than those of p110 $\alpha$ , several have been reported. Many of these are truncations or deletions starting at or near residue 571

(32, 56). In particular, a truncation mutant known as p65 (eliminating all amino acids C-terminal to residue 571), leads to constitutively increased PI3K $\alpha$  activity. It has been proposed that residues 581 to 593 constrain the location of the inhibitory nSH2 domain and that deletion of them removes such orienting constraints (57). On the basis of the crystal structure of p110/niSH2, an alternative possibility appears more likely: Truncation at residue 571 might destabilize the iSH2 coiled-coil around residues 560 and 564 that make an important contact with Asn<sup>345</sup> of the C2 domain. Thus, the effect of this truncation may be equivalent to that of mutation of Asn<sup>345</sup> of the C2 domain discussed above.

**Interaction with the lipid membrane.** Upon activation, PI3Ks are recruited to the plasma membrane, where the phosphatidylinositide substrates reside. A model of the interaction between p110 $\gamma$  and the lipid membrane based on the known location of the active site and the co-crystal structure of p110 $\gamma$  with Ras (50) has been proposed. In this model, loops from the C2 and kinase domains form the major contact sites with the lipid membrane. When this assumed membrane plane is placed in the p110 $\alpha$ /niSH2 structure, the exposed surface of the coiled-coil of iSH2 (residues 447 to 561) forms a long rectangular surface that contacts the putative plane of the membrane. This surface of iSH2, as well as two loops from the kinase domain (residues 723 to 729 and 863 to 867) are rich in basic residues (Lys<sup>447</sup>, Lys<sup>448</sup>, Arg<sup>461</sup>, Arg<sup>465</sup>, Arg<sup>472</sup>, Lys<sup>480</sup>, Lys<sup>530</sup>, Lys<sup>532</sup>, Arg<sup>523</sup>, Arg<sup>534</sup>, Arg<sup>543</sup>, Arg<sup>544</sup>, Lys<sup>551</sup>, and Lys<sup>561</sup> of the iSH2 and Lys<sup>723</sup>, Lys<sup>729</sup>, Lys<sup>863</sup>, and Lys<sup>867</sup> of the kinase domain) and are therefore well-suited for interacting with negatively charged phospholipids (Fig. 3A). The region of iSH2 containing these basic residues thus would appear to be the major determinant of interaction with membranes, in agreement with the observation that iSH2 interacts with phospholipids *in vitro* (58). In contrast, the C2 domain, which had been thought to be the main lipid-interacting domain of p110,

is partly blocked from membrane interaction by iSH2, although it remains possible for the basic residues of its CBR loops (e.g. Arg<sup>349</sup>, Lys<sup>410</sup>, Arg<sup>412</sup>, Lys<sup>413</sup>, Lys<sup>416</sup>) to reach the membrane. Further studies are required to elucidate the relative importance of iSH2 and C2 in lipid membrane interaction.

Ras activates PI3Ks by binding to the RBD of their catalytic subunit. A model of Ras bound to p110 $\alpha$ /niSH2, built by aligning the structure of the Ras-binding domain of p110 $\alpha$  with the structure of the p110 $\gamma$ /Ras complex (50), shows the position of this activator protein in the complex and its relation to the putative membrane plane (Fig. 3B).

The p110 $\alpha$ /niSH2 crystal structure reveals the architecture of the complete catalytic subunit of a class IA PI3K, identifies a contact between the C2 domain of p110 $\alpha$  and iSH2 domain of p85, and suggests a role for iSH2 in lipid binding. It also sheds new light on the mechanisms by which PIK3CA oncogenic mutations affect PI3K $\alpha$  activity. Insights obtained from this structure suggest new targets for the design of isoform- or mutation-specific inhibitors for cancer therapeutics.

#### References and Notes

1. B. Vanhaesebroeck, M. D. Waterfield, *Exp. Cell Res.* **253**, 239 (1999).
2. L. C. Cantley, *Science* **296**, 1655 (2002).
3. T. Maehama, J. E. Dixon, *Trends Cell Biol.* **9**, 125 (1999).
4. B. Vanhaesebroeck, D. R. Alessi, *Biochem. J.* **346**, 561 (2000).
5. B. T. Nave, M. Ouwens, D. J. Withers, D. R. Alessi, P. R. Shepherd, *Biochem. J.* **344**, 427 (1999).
6. B. D. Manning, A. R. Tee, M. N. Logsdon, J. Blenis, L. C. Cantley, *Mol. Cell* **10**, 151 (2002).
7. S. R. Datta *et al.*, *Cell* **91**, 231 (1997).
8. L. del Peso, M. González-García, C. Page, R. Herrera, G. Nuñez, *Science* **278**, 687 (1997).
9. L. D. Mayo, D. B. Donner, *Proc. Natl. Acad. Sci. U.S.A.* **98**, 11598 (2001).
10. B. P. Zhou *et al.*, *Nat. Cell Biol.* **3**, 973 (2001).
11. M. A. Lawlor, P. Rotwein, *Mol. Cell Biol.* **20**, 8983 (2000).
12. L. Rossig *et al.*, *Mol. Cell Biol.* **21**, 5644 (2001).
13. M. H. Cardone *et al.*, *Science* **282**, 1318 (1998).
14. J. A. Romashkova, S. S. Makarov, *Nature* **401**, 86 (1999).
15. A. Brunet *et al.*, *Cell* **96**, 857 (1999).

16. S. Guo *et al.*, *J. Biol. Chem.* **274**, 17184 (1999).
17. G. Rena, S. Guo, S. C. Cichy, T. G. Unterman, P. Cohen, *J. Biol. Chem.* **274**, 17179 (1999).
18. I. Vivanco, C. L. Sawyers, *Nat. Rev. Cancer* **2**, 489 (2002).
19. R. Katso *et al.*, *Annu. Rev. Cell Dev. Biol.* **17**, 615 (2001).
20. A. G. Bader, S. Kang, L. Zhao, P. K. Vogt, *Nat. Rev. Cancer* **5**, 921 (2005).
21. H. W. Chang *et al.*, *Science* **276**, 1848 (1997).
22. J. Li *et al.*, *Science* **275**, 1943 (1997).
23. P. A. Steck *et al.*, *Nat. Genet.* **15**, 356 (1997).
24. I. Sansal, W. R. Sellers, *J. Clin. Oncol.* **22**, 2954 (2004).
25. S. P. Staal, *Proc. Natl. Acad. Sci. U.S.A.* **84**, 5034 (1987).
26. A. Bellacosa *et al.*, *Int. J. Cancer* **64**, 280 (1995).
27. J. Q. Cheng *et al.*, *Proc. Natl. Acad. Sci. U.S.A.* **89**, 9267 (1992).
28. J. Q. Cheng *et al.*, *Proc. Natl. Acad. Sci. U.S.A.* **93**, 3636 (1996).
29. L. Shayesteh *et al.*, *Nat. Genet.* **21**, 99 (1999).
30. B. Actor *et al.*, *Genes Chromosomes Cancer* **34**, 416 (2002).
31. C. B. Knobbe, G. Reifenberger, *Brain Pathol.* **13**, 507 (2003).
32. A. J. Philp *et al.*, *Cancer Res.* **61**, 7426 (2001).
33. Y. Samuels *et al.*, *Science* **304**, 554 (2004).
34. D. K. Broderick *et al.*, *Cancer Res.* **64**, 5048 (2004).
35. K. E. Bachman *et al.*, *Cancer Biol. Ther.* **3**, 772 (2004).
36. J. W. Lee *et al.*, *Oncogene* **24**, 1477 (2005).
37. I. G. Campbell *et al.*, *Cancer Res.* **64**, 7678 (2004).
38. D. A. Levine *et al.*, *Clin. Cancer Res.* **11**, 2875 (2005).
39. L. H. Saal *et al.*, *Cancer Res.* **65**, 2554 (2005).
40. Y. Wang, A. Helland, R. Holm, G. B. Kristensen, A. L. Borresen-Dale, *Hum. Mutat.* **25**, 322 (2005).
41. P. K. Vogt, S. Kang, M. A. Elsliger, M. Gymnopoulos, *Trends Biochem. Sci.* **32**, 342 (2007).
42. S. Kang, A. G. Bader, P. K. Vogt, *Proc. Natl. Acad. Sci. U.S.A.* **102**, 802 (2005).
43. T. Ikenoue *et al.*, *Cancer Res.* **65**, 4562 (2005).
44. A. G. Bader, S. Kang, P. K. Vogt, *Proc. Natl. Acad. Sci. U.S.A.* **103**, 1475 (2006).
45. S. J. Isakoff *et al.*, *Cancer Res.* **65**, 10992 (2005).
46. J. J. Zhao *et al.*, *Proc. Natl. Acad. Sci. U.S.A.* **102**, 18443 (2005).
47. M. Gymnopoulos, M. A. Elsliger, P. K. Vogt, *Proc. Natl. Acad. Sci. U.S.A.* **104**, 5569 (2007).
48. Y. Samuels *et al.*, *Cancer Cell* **7**, 561 (2005).
49. Z. A. Knight, K. M. Shokat, *Biochem. Soc. Trans.* **35**, 245 (2007).
50. M. E. Pacold *et al.*, *Cell* **103**, 931 (2000).
51. E. H. Walker *et al.*, *Mol. Cell* **6**, 909 (2000).
52. E. H. Walker, O. Perisic, C. Ried, L. Stephens, R. L. Williams, *Nature* **402**, 313 (1999).
53. N. Miled *et al.*, *Science* **317**, 239 (2007).
54. R. T. Nolte, M. J. Eck, J. Schlessinger, S. E. Shoelson, S. C. Harrison, *Nat. Struct. Biol.* **3**, 364 (1996).
55. J. Yu, C. Wjasow, J. M. Backer, *J. Biol. Chem.* **273**, 30199 (1998).
56. C. Jimenez *et al.*, *EMBO J.* **17**, 743 (1998).
57. S. C. Shekar *et al.*, *J. Biol. Chem.* **280**, 27850 (2005).
58. P. End *et al.*, *J. Biol. Chem.* **268**, 10066 (1993).
59. Support was provided by the Virginia and D. K. Ludwig Fund for Cancer Research. NIH grants CA 43460 to B.V., GM066895 to L.M.A., and GM07309 and GM 07184 to D.M. Brookhaven National Laboratory is gratefully acknowledged for providing Beamlines X29 and X6a of the National Synchrotron Light Source for collection of the diffraction data. We are grateful to Jr-Ming Yang for the identification of the crystallization condition. Coordinates of the p110 $\alpha$ /nIsh2 have been deposited in the Protein Data Bank (accession number 2RD0, [www.rcsb.org](http://www.rcsb.org)).

#### Supporting Online Material

[www.sciencemag.org/cgi/content/full/318/5857/1744/DC1](http://www.sciencemag.org/cgi/content/full/318/5857/1744/DC1)

Materials and Methods

Figs. S1 to S3

References

21 September 2007; accepted 31 October 2007

10.1126/science.1150799

## REPORTS

# Stored Light in an Optical Fiber via Stimulated Brillouin Scattering

Zhaoming Zhu,<sup>1</sup> Daniel J. Gauthier,<sup>1\*</sup> Robert W. Boyd<sup>2</sup>

We describe a method for storing sequences of optical data pulses by converting them into long-lived acoustic excitations in an optical fiber through the process of stimulated Brillouin scattering. These stored pulses can be retrieved later, after a time interval limited by the lifetime of the acoustic excitation. In the experiment reported here, smooth 2-nanosecond-long pulses are stored for up to 12 nanoseconds with good readout efficiency: 29% at 4-nanosecond storage time and 2% at 12 nanoseconds. This method thus can potentially store data packets that are many bits long. It can be implemented at any wavelength where the fiber is transparent and can be incorporated into existing telecommunication networks because it operates using only commercially available components at room temperature.

An information network consists of nodes where information is generated, processed, routed, and stored, and of transmission links that interconnect the nodes. One bottleneck in modern optical information networks is the lack of an all-optical memory for which the storage time is continuously adjustable (1). Substantial progress has been made in the development of a memory based on spatial-spectral holography (2), but this method requires operation at cryogenic temperatures. Another promising approach is so-called stored or stopped light based on electromagnetically induced transparency (EIT), in which information encoded on an optical beam is impressed upon internal

degrees of freedom of a dense atomic ensemble (3–7). Storage times exceeding 1 s have been observed for a 20- $\mu$ s-long pulse (8), suggesting that this method could be useful as a component in long-distance quantum information networks (9, 10). One limitation of both of these storage methods is that their frequency of operation is highly constrained: The frequency of the stored light must match precisely the resonance frequency of the ions or atoms used. These constraints have been cast aside with the prediction (11) that a pulse can be stored in a dynamically controlled microring resonator containing many narrow resonances over a broad spectral range, and a single optical pulse was stored for  $\sim$ 100 ps in a proof-of-concept experiment (12).

Here, we demonstrate storage of multiple optical pulses by coherently transferring their information content to an acoustic excitation in a room-temperature optical telecommunication fiber through their interaction with an additional

optical “write” pulse. After a controllable storage time, the acoustic excitation is converted back to the optical domain by interaction with a “read” pulse. The process is based on stimulated Brillouin scattering (SBS) (13, 14) and works at any wavelength where the fiber is transparent, including the important telecommunication band in the near-infrared spectral region. The SBS process arises from electrostriction, in which a time-varying electric field creates a time-varying change in density of the material system (i.e., an acoustic excitation). The acoustic wave modulates the refractive index of the medium, which induces both amplifying and absorbing resonances in the vicinity of the applied laser frequencies. Our storage scheme relies on the process of anti-Stokes absorption, which occurs efficiently when the carrier frequency (central frequency) of the incident data pulses is higher than the carrier frequency of the applied write pulse by the Brillouin frequency shift  $\Omega_B$ , which is proportional to the speed of sound in the material and is approximately 9.6 GHz for our fiber at wavelengths near 1.55  $\mu$ m. The SBS process works for data pulses at any carrier frequency so long as the write- and read-pulse frequencies are lower than the data-pulse frequency by  $\Omega_B$ ; this condition can be achieved easily using standard tunable-laser technology.

Our experiment to demonstrate light storage in an optical fiber is conceptually very simple. Bits of information, represented by pulses of light, pass through the fiber while, simultaneously, a write pulse passes through the fiber in the opposite direction (Fig. 1A). Through the process of SBS, essentially all the data-pulse energy is depleted and a coherent acoustic excitation is left behind in the

<sup>1</sup>Duke University, Department of Physics, Box 90305, Durham, NC 27708, USA. <sup>2</sup>The Institute of Optics, University of Rochester, Rochester, NY 14627, USA.

\*To whom correspondence should be addressed. E-mail: [gauthier@phy.duke.edu](mailto:gauthier@phy.duke.edu)